scientific reports

Check for updates

OPEN

The role of a second diffusing component on the Gill–Rees stability problem

B. M. Shankar[1]✉, K. V. Nagamani[1] & I. S. Shivakumara[2]

The stability of natural convection in a vertical porous layer using a local thermal nonequilibrium model was first studied by Rees (Transp Porous Med 87:459–464, 2011) following the proof of Gill (J Fluid Mech 35:545–547, 1969), called the Gill–Rees stability problem. The aim of the present study is to investigate the implication of an additional solute concentration field on the Gill–Rees problem. The stability eigenvalue problem is solved numerically and some novel results not observed in the studies of double-diffusive natural convection in vertical porous (local thermal equilibrium case) and non-porous layers are disclosed. The possibility of natural convection parallel flow in the basic state becoming unstable due to the addition of an extra diffusing component is established. In some cases, the neutral stability curves of stationary and travelling-wave modes are connected to form a loop within which the flow is unstable indicating the requirement of two thermal Darcy–Rayleigh numbers to specify the stability/instability criteria. Moreover, the change in the mode of instability is recognized in some parametric space. The results for the extreme cases of the scaled interphase heat transfer coefficient are discussed.

The stability of natural convection arising due to thermal buoyancy in a porous medium has received considerable attention because of its relevance in various applications such as geophysics, building industry, post-accident heat removal from pebble-bed reactors, modelling of convection in the underground storage of CO_2, the intensification of heat transfer in compact heat exchangers where metal foams are used. The study has remained a subject of active research and the growing volume of work in this area is amply documented in the books by Straughan[1], Nield and Bejan[2] and Barletta[3].

In his seminal paper, Gill[4] proposed rigorous mathematical proof to establish the absence of thermoconvective instability in a differentially heated vertical layer of Darcy porous medium. Other authors further enriched Gill's results by taking into account several aspects such as the inclusion of time derivative term in the momentum equation[5], non-Newtonian fluid behavior[6,7], permeable boundaries[8], Brinkman term[9,10] and the horizontal heterogeneity in permeability[11]. Among these authors, Rees[5], and Barletta and Alves[6] showed that the natural convection parallel flow in the basic state remains stable as propounded by Gill[4]. Whereas, Shankar and Shivakumara[7,11], Barletta[8] and Shankar et al.[9,10] established that the instability of base flow emerges at sufficiently large Darcy–Rayleigh numbers. The usual assumption made in all these studies is that the local thermal equilibrium (LTE) prevails between the solid and fluid phases of the porous medium.

It is expected that LTE will be broken down and the temperatures of solid as well as fluid phases may be no longer identical under highly unsteady conditions, or when the differences between the thermal conductivities of the two phases exist[2]. In such circumstances, one has to utilize the local thermal nonequilibrium (LTNE) model in which two temperature equations, one for the fluid phase and another for the solid phase, are considered with a coupling term in both the equations describing the interphase heat transfer. One of the key issues in dealing with LTNE model is the estimation of the interphase heat transfer coefficient and Rees[12,13] has scrutinized this problem for various classes of materials. The condition of LTE is approached when the coefficient of interphase heat transfer assumes large values. From an application point of view, LTNE model is playing an important role in porous media, such as computer chips via the use of porous metal foams[14,15], drying/freezing of foods[16,17], microwave heating[18] etc. Rees[19] was the first to extend the work of Gill[4] to account LTNE effects and showed that the flow remains stable for all infinitesimal perturbations (hereafter we refer to it as the Gill–Rees stability problem). Scott and Straughan[20] were able to prove that a nonlinear stability analysis, based on the energy method, leads to the same response declared by Gill[1]. Later, Celli et al.[21] reconsidered the analysis carried out by Rees[19] on altering the velocity boundary conditions from the impermeable to permeable and showed numerically the

[1]Department of Mathematics, PES University, Bangalore 560 085, India. [2]Department of Mathematics, Bangalore University, Bangalore 560 056, India. ✉email: bmshankar@pes.edu

possibility of base flow becoming unstable. Further developments on the Gill–Rees problem were taken up by considering viscoelastic effects[22], uniform internal heat generation in both the phases of the porous medium[23] and the combined effects of Darcy–Prandtl number as well as the density maximum property[24]. It was established that instability occurs in all these cases under certain conditions.

In some practical problems encountered in nature and in the industry, such as in devising an effective method of disposing of waste material and extraction of energy, some dissolved substance may exist in addition to temperature contributing in opposite senses to the buoyancy gradient.The instability occurring due to this process is known as thermosolutal convection or double-diffusive convection. The comprehensive literature existing on double-diffusive convection in porous media is well documented in the books by Straughan[25] and Nield and Bejan[2]. Nonetheless, the stability of double-diffusive natural convection in a vertical porous layer has not received due attention in the literature and it is in the much-to-be desired state. Inspired by the pioneering paper by Gershuni et al.[26], a few authors have analyzed the stability of convective flow of a binary mixture in a vertical porous layer and, in particular, this work was examined for all values of the Darcy–salinity Rayleigh number by Khan and Zebib[27]. It was found that for salinity Rayleigh number $R_S < 7.901$ there are no two-dimensional instabilities, however, instability sets in via stationary mode for $R_S \geq 7.901$. The stability of natural convection induced by buoyancy due to temperature and solute concentration fields in a vertical porous layer was investigated in detail by Shankar et al.[28]. It was observed that there exists a solute Darcy–Rayleigh number space within which the flow gets destabilized and beyond which it stabilizes reversely depending on the values of the Lewis number. The above studies were mainly based on the assumption that the fluid and porous-medium phases are everywhere in LTE.

As propounded by the previous studies, the consideration of LTNE model in the study of heat and mass transfer in a porous medium is of paramount importance. In a porous medium, heat is shared between the fluid and the solid skeleton and thus the process is double-advective while the solute concentration is confined only to the pore space. Moreover, the thermal signals are advected more slowly than solute concentration signals, and this difference in advection rates may be crucial to the stability aspects of the system[29]. The aim of this paper is to explore the influence of an additional diffusing component on the Gill–Rees stability problem. More precisely, the stability of thermosolutal convection in a vertical porous layer is studied numerically using a LTNE model. The two end vertical boundaries are assumed to be impermeable and maintained at unequal uniform temperatures and solute concentrations. Within this more general scheme, the prediction of instability is validated through a stability eigenvalue problem derived by adopting a modal analysis. The effect of additional diffusing component is discussed for the neutral stability curves and the critical values of the wavenumber and of the thermal Darcy–Rayleigh number.

Statement of the problem and governing equations

A vertical porous layer of thickness $2L$ is considered wherein the two end vertical impermeable walls are maintained at uniform but different temperatures T_1 and T_2, with $T_2 > T_1$ and solute concentrations C_1 and C_2, with $C_2 > C_1$. A Cartesian reference frame (x^*, y^*, z^*) is chosen so that the x^*-axis is horizontal and perpendicular, y^*-axis is horizontal and parallel, while the z^*-axis is vertical and parallel to the porous channel. The origin of the axes is in the middle of the porous layer and the acceleration due to gravity $\vec{g} = -g\hat{k}$, where $\hat{k}$ is the unit vector in the vertical z^*-direction. A sketch of the porous channel cross-section in the x^*z^*-plane is shown in Fig. 1. The porous medium is considered to be homogeneous, isotropic and the LTNE model is invoked with two temperature equations, one for the fluid phase and another for the solid phase. The fluid density ρ_f varies linearly with fluid temperature T_f^* and the solute concentration C^* of the dissolved species in the form

$$\rho_f\left(T_f^*, C^*\right) = \rho_0\left\{1 - \beta_T\left(T_f^* - T_0\right) + \beta_S\left(C^* - C_0\right)\right\}, \tag{1}$$

where β_T is the volumetric thermal expansion coefficient, β_S is the solute expansion coefficient, $T_0 = (T_1 + T_2)/2$ is the reference temperature, $C_0 = (C_1 + C_2)/2$ is the reference solute concentration and $\rho_0 = \rho_f(T_0, C_0)$. The starred symbols denote the dimensional variables. The dimensionless dependent variables $\left(\vec{q}, T_f, T_s, C, P\right)$, space coordinates (x, y, z) and time t are defined as follows:

$$\vec{q}^*\frac{L}{\varepsilon\kappa_f} = \vec{q}, \frac{\left(T_{f,s}^* - T_0\right)}{(T_2 - T_1)} = T_{f,s}, \frac{(C^* - C_0)}{(C_2 - C_1)} = C, P^*\frac{K}{\varepsilon\kappa_f\mu} = P, \left(x^*, y^*, z^*\right)\frac{1}{L} = \left(x, y, z\right), t^*\frac{\kappa_f}{L^2} = t, \tag{2}$$

where $\kappa_f = k_f/(\rho c)_f, k_f, (\rho c)_f, \vec{q} = (u, v, w)$, P, ε, K, μ and T_s are the effective thermal diffusivity of the fluid, thermal conductivity of the fluid, heat capacity of the fluid, seepage velocity vector, dynamic pressure, porosity, permeability, fluid viscosity and temperature of the solid phase, respectively. Since two-dimensional motion is more unstable than three-dimensional, the stream function $\psi(x, z, t)$ is introduced through $u = -\partial\psi/\partial z$ and $w = \partial\psi/\partial x$. Thus, the dimensionless governing equations under the Oberbeck–Boussinesq approximation and the relevant boundary conditions are Rees[19] and Shankar et al.[28]

$$\frac{\partial^2\psi}{\partial x^2} + \frac{\partial^2\psi}{\partial z^2} = R_D\frac{\partial T_f}{\partial x} - R_S\frac{\partial C}{\partial x}, \tag{3}$$

$$\frac{\partial T_f}{\partial t} + \frac{\partial\psi}{\partial x}\frac{\partial T_f}{\partial z} - \frac{\partial\psi}{\partial z}\frac{\partial T_f}{\partial x} = \frac{\partial^2 T_f}{\partial x^2} + \frac{\partial^2 T_f}{\partial z^2} + H\left(T_s - T_f\right), \tag{4}$$

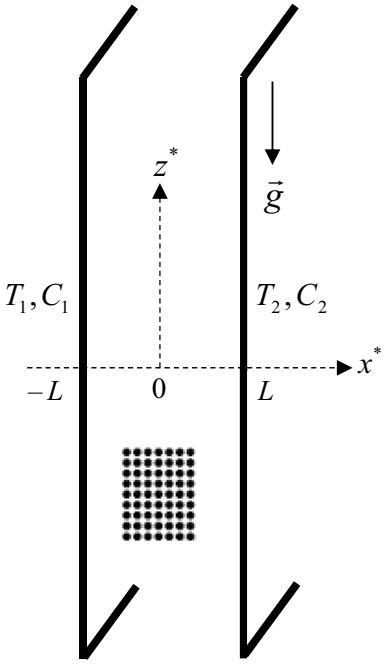

Figure 1. A sketch of the vertical porous layer.

$$\alpha \frac{\partial T_s}{\partial t} = \frac{\partial^2 T_s}{\partial x^2} + \frac{\partial^2 T_s}{\partial z^2} - H\gamma\left(T_s - T_f\right), \tag{5}$$

$$\frac{\partial C}{\partial t} + \frac{\partial \psi}{\partial x}\frac{\partial C}{\partial z} - \frac{\partial \psi}{\partial z}\frac{\partial C}{\partial x} = \frac{1}{Le}\left(\frac{\partial^2 C}{\partial x^2} + \frac{\partial^2 C}{\partial z^2}\right), \tag{6}$$

$$\psi = 0 \,\text{at}\, x = \pm 1,\ T_f = T_s = C = -1/2 \,\text{at}\, x = -1,\ T_f = T_s = C = 1/2 \,\text{at}\, x = 1. \tag{7}$$

In the above equations, $R_D = \rho_0 g \beta_T (T_2 - T_1) KL/\varepsilon\mu\kappa_f$ is the thermal Darcy–Rayleigh number, $R_S = \rho_0 g \beta_s (C_2 - C_1) KL/\varepsilon\mu\kappa_f$ is the solutal Darcy–Rayleigh number, $H = hL^2/\varepsilon k_f$ is the scaled interphase heat transfer coefficient, $\gamma = \varepsilon k_f/(1-\varepsilon)k_s$ is the ratio of porosity-modified thermal conductivities, $\alpha = (\rho c)_s k_f/(\rho c)_f k_s = \kappa_f/\kappa_s$ is the ratio of thermal to solid diffusivities and $Le = \kappa_f/\kappa_c$ is the Lewis number, while h is the interphase heat transfer coefficient, k_s is the thermal conductivity of the solid, $(\rho c)_s$ is the heat capacity of the solid and κ_c is the solute concentration diffusivity.

Base flow

A basic flow solution driven by both thermal and solutal buoyancy forces is obtained in a stationary regime with $\psi = \psi_b(x)$, $T_f = T_{fb}(x), T_s = T_{sb}(x)$ and $C = C_b(x)$ in the form

$$\psi_b(x) = \left(1/4\right)(R_D - R_S)(x^2 - 1), T_{fb}(x) = T_{sb}(x) = C_b(x) = x/2. \tag{8}$$

Linear stability analysis

Following the usual approach of the linearized theory of hydrodynamic stability, perturbations are introduced on the basic state in the form

$$\psi = \psi_b(x) + \hat{\psi}(x,z,t), T_f = T_{fb}(x) + \hat{T}_f(x,z,t), T_s = T_{sb}(x) + \hat{T}_s(x,z,t), C = C_b(x) + \hat{C}(x,z,t), \tag{9}$$

where the hat above a quantity designates the perturbation field. Substituting Eq. (9) into the above governing equations, neglecting the nonlinear terms and seeking the solution via the standard Fourier decomposition

$$\left(\psi, T_f, T_s, C\right) = [\Psi, \Theta, \Phi, \Gamma] e^{ia(z-ct)}, \tag{10}$$

where the quantities Ψ, Θ, Φ and Γ are the complex amplitude functions of x, a is the wave number in the z -direction and $c(= c_r + ic_i)$ is the complex wave speed, we obtain the disturbance stability equations in the form

$$\left(D^2 - a^2\right)\Psi - R_D D\Theta + R_S D\Gamma = 0, \tag{11}$$

$$-\left(ia/2\right)\{(R_D - R_S)x\Theta - \Psi\} + \left(D^2 - a^2\right)\Theta + H(\Phi - \Theta) = -iac\,\Theta, \tag{12}$$

$$\left(D^2 - a^2\right)\Phi - H\gamma(\Phi - \Theta) = -iac\,\alpha\,\Phi, \tag{13}$$

$$-\left(ia/2\right)\{(R_D - R_S)x\Gamma - \Psi\} + \frac{1}{Le}\left(D^2 - a^2\right)\Gamma = -iac\,\Gamma, \tag{14}$$

where D denotes differentiation with respect to x. We note that the flow is stable or unstable for $c_i < 0$ or $c_i > 0$ and neutrally stable for $c_i = 0$.

The associated boundary conditions are

$$\Psi = \Phi = \Theta = \Gamma = 0 \text{ at } x = \pm 1. \tag{15}$$

Gill–Rees growth rate analysis

In this section, we attempt to determine the sign of the growth rate c_i using the integral method employed by Gill[4] and Rees[19]. First, we operate $(D^2 - a^2)$ on Eqs. (12), (13) and (14) and make use of Eq. (11) to eliminate Ψ, and get

$$\begin{aligned}&\left(\Theta'''' + a^4\Theta - 2a^2\Theta''\right) + H\left(\Phi'' - a^2\Phi\right) - H\left(\Theta'' - a^2\Theta\right) - \frac{iaR_D}{2}\left(\left(x\Theta'\right)' - a^2x\Theta\right)\\ &\quad + \frac{iaR_S}{2}\left((x\Theta)'' - \Gamma' - a^2x\Theta\right) = -iac\left(\Theta'' - a^2\Theta\right),\end{aligned} \tag{16}$$

$$\left(\Phi'''' + a^4\Phi - 2a^2\Phi''\right) + H\gamma\left(\Theta'' - a^2\Theta\right) - H\gamma\left(\Phi'' - a^2\Phi\right) = -ia\alpha c\left(\Phi'' - a^2\Phi\right), \tag{17}$$

$$\frac{1}{Le}\left(\Gamma'''' + a^4\Gamma - 2a^2\Gamma''\right) - \frac{iaR_D}{2}\left((x\Gamma)'' - \Theta' - a^2x\Gamma\right) + \frac{iaR_S}{2}\left(\left(x\Gamma'\right)' - a^2x\Gamma\right) = -iac\left(\Gamma'' - a^2\Gamma\right). \tag{18}$$

We multiply Eq. (16) by $\gamma\,\overline{\Theta}$, Eq. (17) by $\overline{\Phi}$ and Eq. (18) by $\overline{\Gamma}$, where the bar over the symbol denotes complex conjugate. Then, we integrate over $-1 \le x \le 1$ and add the resulting equations to get

$$\begin{aligned}&\gamma\int_{-1}^{1}\left(\Theta''''\overline{\Theta} + a^4|\Theta|^2 - 2a^2\Theta''\overline{\Theta}\right)dx + H\gamma\int_{-1}^{1}\left(\Phi''\overline{\Theta} - a^2\Phi\overline{\Theta}\right)dx - H\gamma\int_{-1}^{1}\left(\Theta''\overline{\Theta} - a^2|\Theta|^2\right)dx\\ &\quad - \frac{ia\gamma R_D}{2}\int_{-1}^{1}\left[\left(x\Theta'\right)'\overline{\Theta} - a^2x|\Theta|^2\right]dx + \frac{ia\gamma R_S}{2}\int_{-1}^{1}\left[(x\Theta)''\overline{\Theta} - \Gamma'\overline{\Theta} - a^2x|\Theta|^2\right]dx\\ &\quad + \int_{-1}^{1}\left(\Phi''''\overline{\Phi} + a^4|\Phi|^2 - 2a^2\Phi''\overline{\Phi}\right)dx + H\gamma\int_{-1}^{1}\left(\Theta''\overline{\Phi} - a^2\Theta\overline{\Phi}\right)dx - H\gamma\int_{-1}^{1}\left(\Phi''\overline{\Phi} - a^2|\Phi|^2\right)dx\\ &\quad + \frac{1}{Le}\int_{-1}^{1}\left(\Gamma''''\overline{\Gamma} + a^4|\Gamma|^2 - 2a^2\Gamma''\overline{\Gamma}\right)dx - \frac{iaR_D}{2}\int_{-1}^{1}\left[(x\Gamma)''\overline{\Gamma} - \Theta'\overline{\Gamma} - a^2x|\Gamma|^2\right]dx\\ &\quad + \frac{iaR_S}{2}\int_{-1}^{1}\left[\left(x\Gamma'\right)'\overline{\Gamma} - a^2x|\Gamma|^2\right]dx = -iac\int_{-1}^{1}\left[\gamma\left(\Theta''\overline{\Theta} - a^2|\Theta|^2\right) + \alpha\left(\Phi''\overline{\Phi} - a^2|\Phi|^2\right) + \left(\Gamma''\overline{\Gamma} - a^2|\Gamma|^2\right)\right]dx.\end{aligned} \tag{19}$$

We now manipulate Eq. (19) by performing the integration by parts and using the boundary conditions. This procedure gives

$$\gamma\int_{-1}^{1}\left(\left|\Theta''\right|^2+a^4|\Theta|^2+2a^2\left|\Theta'\right|^2\right)dx+H\gamma\int_{-1}^{1}\left(\left|\Theta'-\Phi'\right|^2+a^2|\Theta-\Phi|^2\right)dx$$
$$+\frac{ia}{2}(R_D-R_S)\int_{-1}^{1}x\left[\gamma\left(\left|\Theta'\right|^2+a^2|\Theta|^2\right)+\left(\left|\Gamma'\right|^2+a^2|\Gamma|^2\right)\right]dx+\frac{iaR_D}{2}\int_{-1}^{1}(\Theta'-\Gamma')\overline{\Gamma}dx$$
$$-\frac{ia\gamma R_S}{2}\int_{-1}^{1}(\Gamma'-\Theta')\overline{\Theta}dx+\int_{-1}^{1}\left(\left|\Phi''\right|^2+a^4|\Phi|^2+2a^2\left|\Phi'\right|^2\right)dx+\frac{1}{Le}\int_{-1}^{1}\left(\left|\Gamma''\right|^2+a^4|\Gamma|^2+2a^2\left|\Gamma'\right|^2\right)dx$$
$$=iac\int_{-1}^{1}\left[\gamma\left(\left|\Theta'\right|^2+a^2|\Theta|^2\right)+\alpha\left(\left|\Phi'\right|^2+a^2|\Phi|^2\right)+\left(\left|\Gamma'\right|^2+a^2|\Gamma|^2\right)\right]dx, \tag{20}$$

where

$$\left|\Theta'-\Phi'\right|^2=\left|\Theta'\right|^2+\left|\Phi'\right|^2-\Phi'\overline{\Theta}'-\Theta'\overline{\Phi}',|\Theta-\Phi|^2=|\Theta|^2+|\Phi|^2-\Phi\overline{\Theta}-\Theta\overline{\Phi}. \tag{21}$$

The fourth and fifth terms on the left-hand side of Eq. (20) discard the possibility of arriving at any definite conclusion in deciding the sign of c_i as it may be positive or negative. This is another instance wherein the Gill–Rees method of proving the stability of fluid flow becomes ineffective. For a single component system ($R_S=0$), however, the above equation simply reduces to

$$\gamma\int_{-1}^{1}\left(\left|\Theta''\right|^2+a^4|\Theta|^2+2a^2\left|\Theta'\right|^2\right)dx+H\gamma\int_{-1}^{1}\left(\left|\Theta'-\Phi'\right|^2+a^2|\Theta-\Phi|^2\right)dx$$
$$+\frac{ia\gamma R_D}{2}\int_{-1}^{1}x\left(\left|\Theta'\right|^2+a^2|\Theta|^2\right)dx+\int_{-1}^{1}\left(\left|\Phi''\right|^2+a^4|\Phi|^2+2a^2\left|\Phi'\right|^2\right)dx \tag{22}$$
$$=iac\int_{-1}^{1}\left[\gamma\left(\left|\Theta'\right|^2+a^2|\Theta|^2\right)+\alpha\left(\left|\Phi'\right|^2+a^2|\Phi|^2\right)\right]dx.$$

Equating the real part on both sides of the above equation allows one to conclude that c_i is always strictly negative for all infinitesimal perturbations. Hence, the basic state is asymptotically stable and this conclusion is in conformity with Rees's proof of stability[19]. The lack of formal proof of stability due to the presence of an additional diffusing component leaves an open possibility to investigate the stability or instability of the basic flow through a numerical solution.

Numerical procedure

The Chebyshev collocation method is used to solve the eigenvalue problem constituted by Eqs. (11)–(15). The Chebyshev polynomial of *kth* order is given by

$$\xi_k(x)=\cos(k\cos^{-1}x), \tag{23}$$

with collocation points

$$x_j=\cos\left(\frac{\pi j}{N}\right),\quad j=0,1,2,\ldots,N, \tag{24}$$

where N is the number of Chebyshev polynomials. Here, $j=0$ and N correspond to the right and left wall boundaries, respectively. The field variables Ψ, Θ, Φ and Γ are approximated in terms of the Chebyshev variable as follows

$$\Psi(x)=\sum_{j=0}^{N}\Psi_j\xi_j(x),\Theta(x)=\sum_{j=0}^{N}\Theta_j\xi_j(x),\Phi(x)=\sum_{j=0}^{N}\Phi_j\xi_j(x),\Gamma(x)=\sum_{j=0}^{N}\Gamma_j\xi_j(x), \tag{25}$$

where Ψ_j, Θ_j, Φ_j and Γ_j are constants. Equations (11)-(15) are discretized in terms of Chebyshev polynomials to get

$$\left(\sum_{k=0}^{N}B_{jk}\Psi_k-a^2\Psi_j\right)-R_D\sum_{k=0}^{N}A_{jk}\Theta_k+R_S\sum_{k=0}^{N}A_{jk}\Gamma_k=0, \tag{26}$$

$$-\left(ia/2\right)\left\{(R_D-R_S)x_j\Theta_j-\Psi_j\right\}+\left(\sum_{k=0}^{N}B_{jk}\Theta_k-a^2\Theta_j\right)+H(\Phi_j-\Theta_j)=-iac\Theta_j, \tag{27}$$

$$\left(\sum_{k=0}^{N}B_{jk}\Phi_k-a^2\Phi_j\right)-H\gamma(\Phi_j-\Theta_j)=-ia\alpha c\Phi_j, \tag{28}$$

$$-\left(ia/2\right)\left\{(R_D-R_S)x_j\Gamma_j-\Psi_j\right\}+\frac{1}{Le}\left(\sum_{k=0}^{N}B_{jk}\Gamma_k-a^2\Gamma_j\right)=-iac\Gamma_j, \tag{29}$$

$$\Psi_0=\Psi_N=0,\ \Theta_0=\Theta_N=0,\ \Phi_0=\Phi_N=0,\ \Gamma_0=\Gamma_N=0, \tag{30}$$

where

$$A_{00}=\frac{\left(2N^2+1\right)}{6}=-A_{NN},\ A_{jk}=\frac{c_j(-1)^{k+j}}{c_k(x_j-x_k)};\ j\neq k, A_{jk}=-\frac{x_j}{2(1-x_j^2)};\ 1\leq k=j\leq N-1,$$
$$B_{jk}=A_{jm}\cdot A_{mk}, \tag{31}$$

with

$$c_j=\begin{cases}1 & 1\leq j\leq N-1\\ 2 & j=0,N\end{cases}. \tag{32}$$

Equations (26)–(30) lead to a generalized eigenvalue problem of the form

$$AX=cBX, \tag{33}$$

where A and B are square complex matrices of order $4(N+1)$, c is the eigenvalue and X is the eigenfunction. For fixed values of governing parameters $R_S,\ H,\ \gamma, \alpha, Le$ and a the value of c_r at which $c_i=0$ is found by varying R_D, which is accomplished by the secant method for a fixed point determination. In accomplishing this we have selected the eigenvalue having the largest imaginary part. Repeating this procedure for different values of a, the marginal stability curve is obtained, say $R_D^*(a, R_S,\ H,\ \gamma, \alpha, Le)$ and the corresponding frequency $c_r^*(a, R_S,\ H,\ \gamma, \alpha, Le)$. The critical values $R_{Dc}(a_c, R_S,\ H,\ \gamma, \alpha, Le)=\min R_D^*(a, R_S,\ H,\ \gamma, \alpha, Le)$ and $c_c(a_c, R_S,\ H,\ \gamma, \alpha, Le)$ are then obtained for specified values of $R_S,\ H,\ \gamma, \alpha$ and Le[30,31]. If $c_c=0$ then the critical disturbance modes are stationary otherwise they are travelling-waves. It should be noted that $R_{Dc}=\min\left(R_{Dc}^S, R_{Dc}^T\right)$ if both the modes exist, where R_{Dc}^S and R_{Dc}^T are the critical thermal Darcy–Rayleigh numbers for the stationary and the travelling-wave modes, respectively.

The convergence of the numerical scheme used is tested by evaluating the response of the number of collocation points N on the critical stability parameters for different sets of governing parameters. The computed values so obtained are tabulated in Table 1 and it is seen that the accuracy improves as N increases. Regardless of the values of the governing parameters, the critical values for distinct values of N exceeding 14 are identical up to 5 decimal places. Therefore, all of the computations are reported by taking $N=15$.

Results and discussion

The Gill–Rees stability problem is extended to capture the influence of a second diffusing component which has precluded the possibility of proving the stability of base flow analytically. The eigenvalue problem is solved numerically using the Chebyshev collocation method. The present problem contains six parameters such as the Darcy–Rayleigh number R_D, the solutal Darcy–Rayleigh number R_S, the Lewis number Le, the scaled interphase heat transfer coefficient H, the porosity modified thermal conductivities ratio γ and the ratio of thermal diffusivities α. The results are presented in terms of critical values of R_D computed with respect to the wave number a for various values of R_S, Le, H and γ assuming α to be unity. To explore the several limiting cases, the parameters are considered in the ranges, $H\in\left[10^{-5}, 10^4\right]$, $\gamma\in\left[10^{-2}, 10\right]$, $R_S\in[0, 2000]$ and the Lewis number is chosen in the range 0.1–10[32].

Growth rate analysis. The growth rate of normal modes is pursued by computing the complex eigenvalue c_r+ic_i for the assigned governing parameters. The most essential information regarding the stable/unstable behavior of the basic flow comes from the sign of the growth rate c_i. Plots of c_i versus the wave number a for different values of H, R_D and γ when $R_S=0$ are reported in Fig. 2a–c. The numerical data reported in these figures support the conclusion that c_i is negative in every case suggesting that no instability is possible. This result agrees with the analytical proof presented by Rees[19]. Nonetheless, the results portrayed for $R_S\neq 0$ in Fig. 3a–e demonstrate the possibility of c_i undergoing a transition from negative to positive with increasing a. This indicates the chances of base flow becoming unstable in the presence of a second diffusing component depending on the values of governing parameters. A closer look at these figures also reveals that larger values of R_D (Fig. 3a), R_S (Fig. 3b) and Le (Fig. 3c), while smaller values of H(Fig. 3d) and γ (Fig. 3e) are necessary for c_i to be positive.

	$R_S = 500,\ \gamma = 1,\ Le = 0.5, H = 1$			$R_S = 1000,\ \gamma = 1,\ Le = 0.5, H = 1$			$R_S = 500,\ \gamma = 1,\ Le = 0.5, H = 100$			$R_S = 500,\ \gamma = 10,\ Le = 0.5, H = 1$			$R_S = 500,\ \gamma = 1,\ Le = 10, H = 1$		
N	R_{Dc}	a_c	c_c	R_{Dc}	a_c	c_c	R_{Dc}	a_c	c_c	R_{Dc}	a_c	c_c	R_{Dc}	a_c	c_c
3	455.15806	0.569400	0	904.16424	0.290263	0	458.54404	1.304487	± 9.624306	445.32753	0.449990	0	127.51952	2.236738	± 89.312561
4	416.98237	0.355783	0	829.30129	0.176603	0	487.79367	1.318743	± 9.639258	397.68067	0.286170	0	347.89680	0.279217	± 18.969205
6	413.72210	0.326146	0	824.03654	0.161680	0	477.92587	1.191875	± 10.015439	396.15973	0.263758	0	300.92250	1.057651	± 58.751588
8	413.59792	0.326841	0	823.73027	0.162086	0	478.10165	1.188263	± 9.954005	395.81154	0.264629	0	342.99234	1.226615	± 41.552617
10	413.56882	0.326854	0	823.67317	0.162092	0	478.12514	1.188081	± 9.952649	395.78540	0.264643	0	348.15457	1.715510	± 11.466295
11	413.57079	0.326850	0	823.67705	0.162091	0	478.12542	1.188079	± 9.952635	395.78690	0.264642	0	352.19606	2.164755	0
12	413.56977	0.326855	0	823.67495	0.162093	0	478.12567	1.188075	± 9.952608	395.78597	0.264645	0	359.16319	2.750712	± 9.071511
13	413.56964	0.326856	0	823.67470	0.162093	0	478.12576	1.188076	± 9.952607	395.78587	0.264646	0	352.87541	0.028388	0
14	413.56969	0.326856	0	823.67480	0.162093	0	478.12578	1.188076	± 9.952605	395.78592	0.264645	0	352.87541	0.028388	0
15	413.56969	0.326856	0	823.67480	0.162093	0	478.12578	1.188076	± 9.952605	395.78592	0.264645	0	352.87541	0.028388	0

Table 1. Convergence tests of the Chebyshev collocation method for representative values of governing parameters.

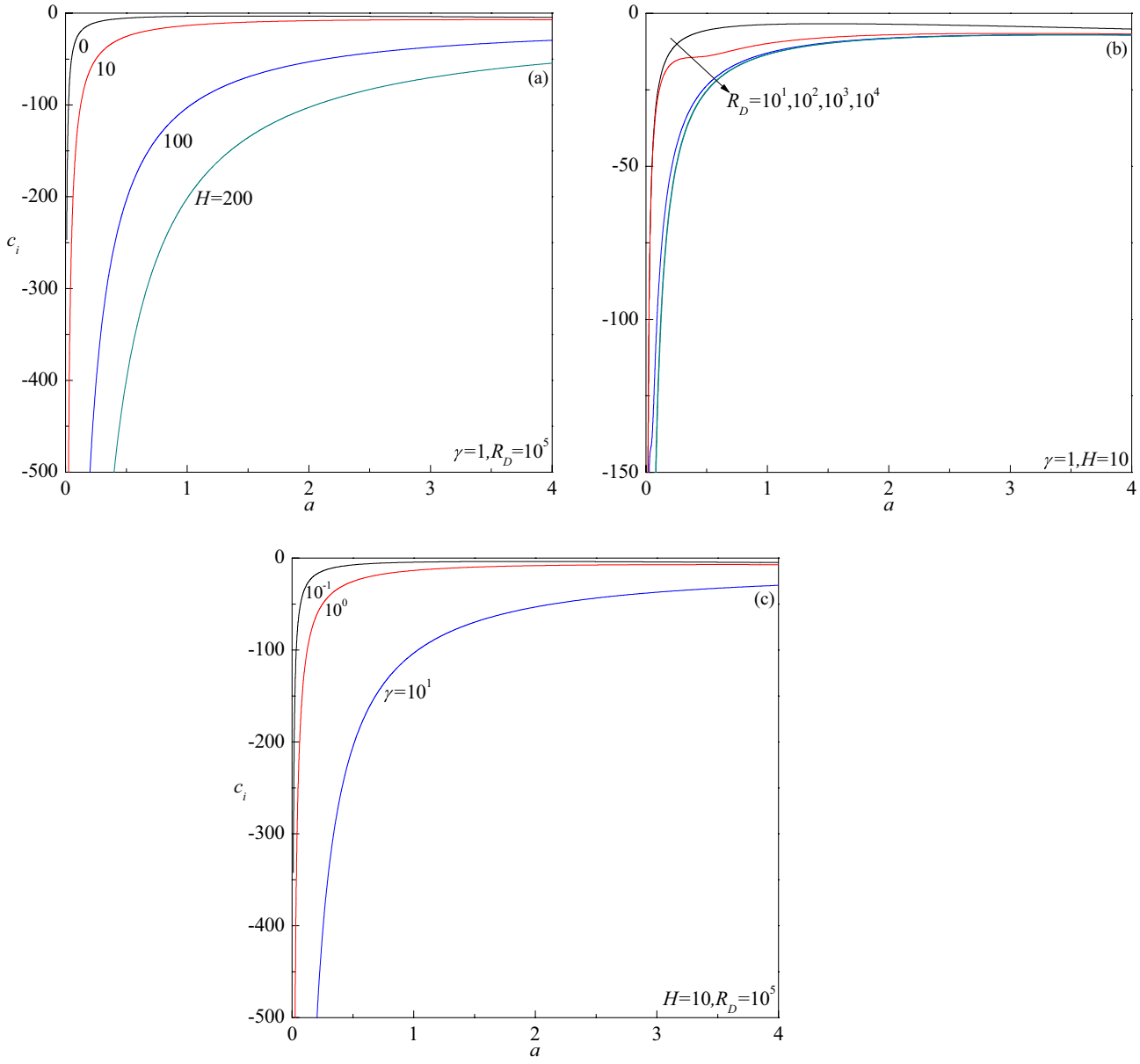

Figure 2. Growth rate c_i versus a for different values of (**a**) H, (**b**) R_D and (**c**) Le, in the absence of a second-diffusing component ($R_S = 0$).

Neutral stability curves. A systematic study on the topology of neutral stability curves is carried out. The neutral stability curve which delimits the boundary between the regions of parametric stability and instability is generated by specifying a vanishing growth rate ($c_i = 0$) of the perturbation modes. Figure 4a–d display the neutral stability curves for different values of R_S, H, Le and γ. Some novel consequences not perceived either in double-diffusive vertical porous (LTE model) or non-porous domains are found for certain choices of parametric values. The neutral stability curves form a loop comprising both stationary and travelling-wave modes, in some cases, exhibiting a local minimum of their own and the least among the two determines the nature of instability mode. The region inside the loop corresponds to instability ($c_i > 0$) and the outside defines the parametric conditions of linear stability ($c_i < 0$). This indicates the requirement of two values of the thermal Darcy–Rayleigh number to specify the linear instability criteria.

Figure 4a shows the evolution of neutral stability curves for different values of R_S when $\gamma = 1$, $Le = 2$ and $H = 100$. For $R_S = 1000$, it is seen that the closed neutral curve consists of travelling-wave mode, which is connected on either side by those of stationary mode; an unusual phenomenon not observed in the earlier studies of double-diffusive convection[28,33]. While both the modes exhibit local minimum, the least among the two corresponds to the travelling-wave mode which dominates the mode of instability. Although a similar trend exists for $R_S = 300$, the instability region gets reduced and the mode of instability turns out to be stationary in this case. At $R_S = 100$, the instability region gets further diminished. Moreover, the neutral curve of travelling-wave mode appears only in the upper portion of the loop confining to a smaller range of wave number a and the preferred

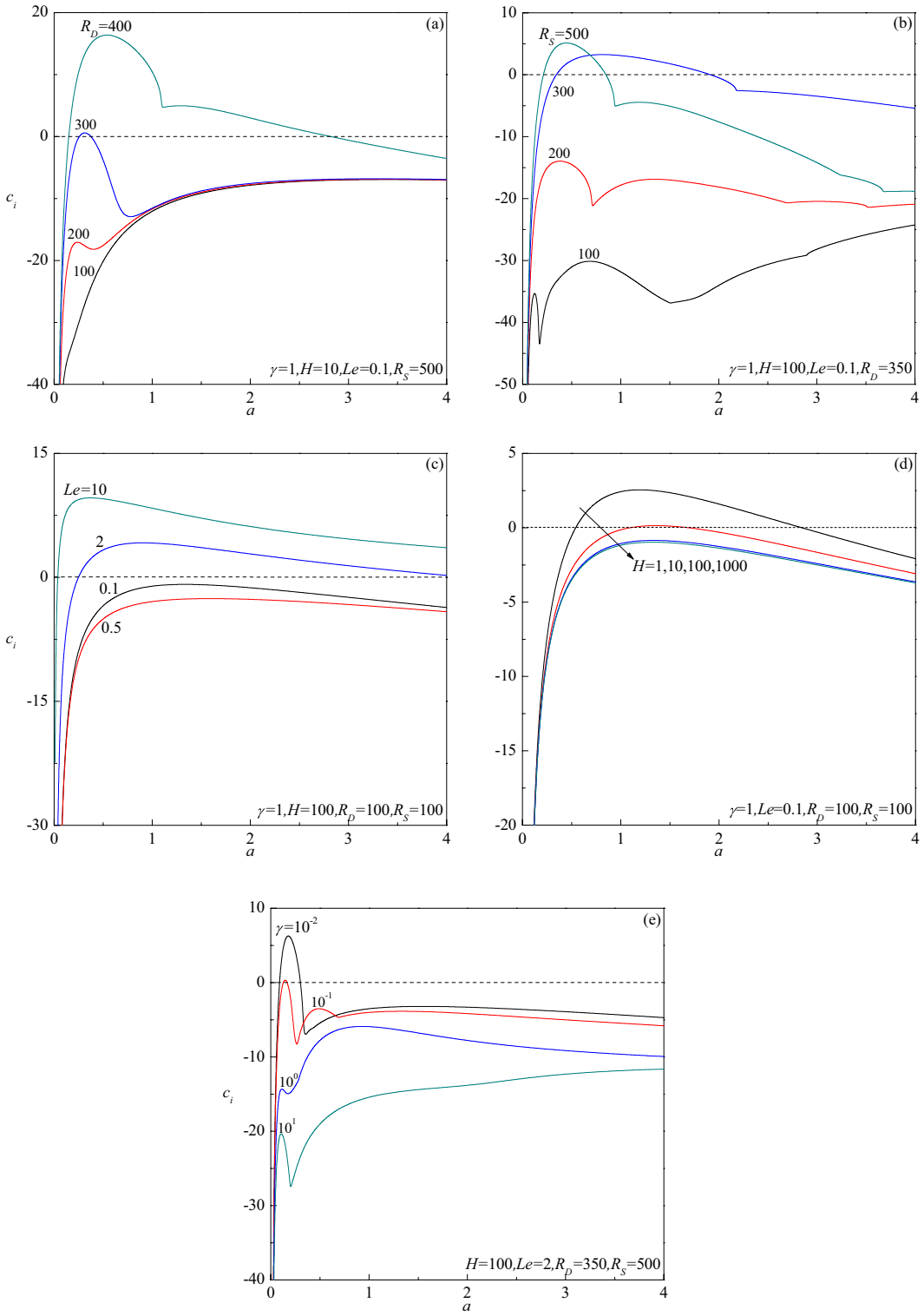

Figure 3. Growth rate c_i versus a for different values of (**a**) R_D, (**b**) R_S, (**c**) Le, (**d**) H and (**e**) γ.

mode of instability remains to be stationary. The region of instability continues to diminish for $R_S = 89$ and 33 and now the closed loop consists only of the neutral curve of stationary mode. The region of instability eventually disappears with a further decrease in the value of R_S because the perturbations exhibit a negative growth rate.

Figure 4b–d exhibit the way in which the neutral curves evolve for different values of H (with $\gamma = 1$, $Le = 2, R_S = 400$), Le (with $\gamma = 1$, $H = 100$, $R_S = 400$) and γ (with $H = 100$, $Le = 2, R_S = 400$), respectively. The outline of neutral curves is akin to those identified in Fig. 4a. It is seen that the effect of increasing H and Le as well as decreasing γ is to enlarge the size of the instability region. For $H = 0.1$ and 20, the instability

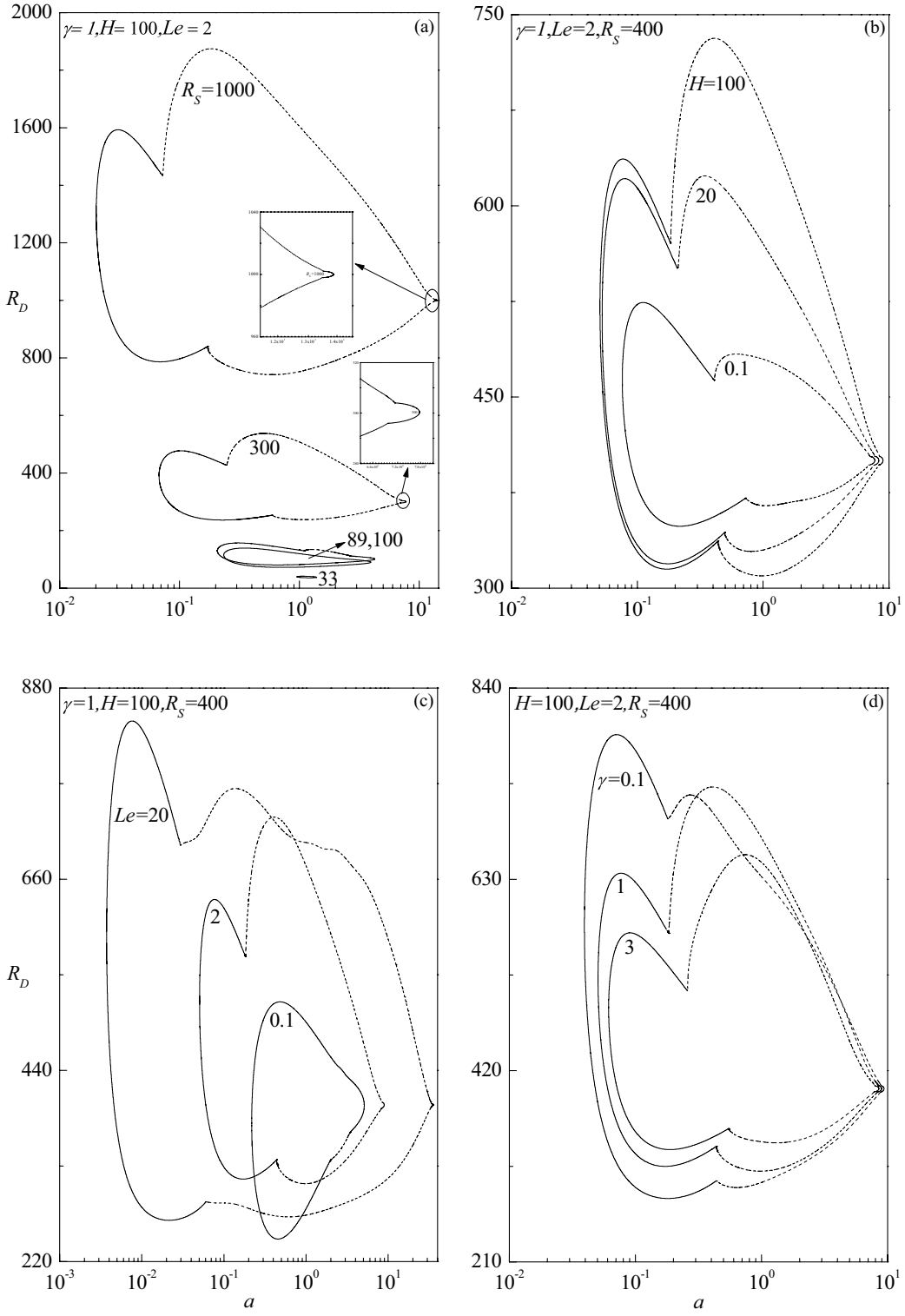

Figure 4. Evolution of neutral stability curves in the (a, R_D)-plane for different values of (**a**) R_S, (**b**) H, (**c**) Le and (**d**) γ. The solid and dashed lines respectively denote the stationary and travelling-wave modes. This convention applies to all the figures hereafter.

occurs through the stationary mode, while for $H = 100$ it switches over to the travelling-wave mode (Fig. 4b). The pattern of instability keeps shifting between the stationary and travelling-wave modes with increasing Le (Fig. 4c) and γ (Fig. 4d). The sensitivity of governing parameters on the progression of neutral curves is examined

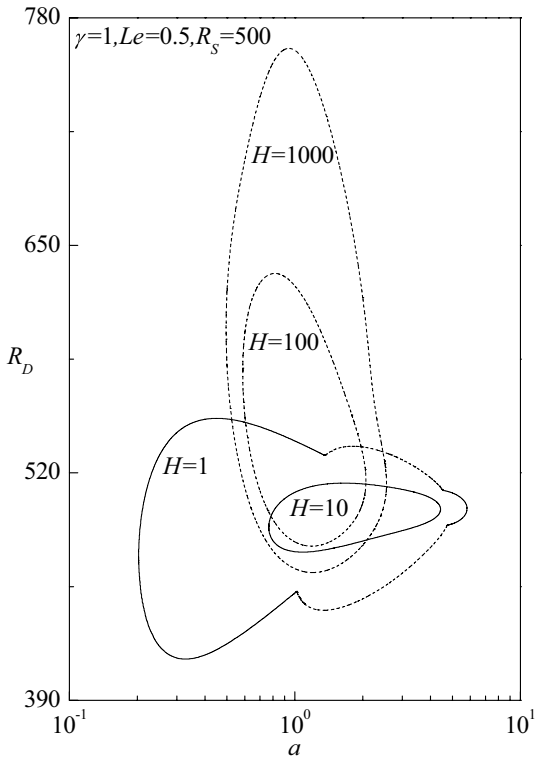

Figure 5. Evolution of neutral stability curves in the (a, R_D)-plane for different values of H.

and displayed in Fig. 5 for various values of H when $\gamma = 1$, $Le = 0.5$ and $R_S = 500$. The neutral curve loop includes both stationary and travelling-wave modes for $H = 1$ as noted earlier, while for $H = 10$ it consists of only stationary mode but for $H = 100$ and 1000 it consists of only travelling-wave mode. Thus, increase in H is to alter the mode of instability from the stationary to the travelling-wave mode. In addition, the instability region corresponding to the travelling-wave mode gets elongated vertically with increasing H.

Stability boundaries. The critical thermal Darcy–Rayleigh number R_{Dc}, the corresponding critical wave number a_c and the critical wave speed c_c, are computed for different values of governing parameters to know their impact on the stability of fluid flow. The trend of R_{Dc} with H for different values of R_S is shown in Fig. 6a–d for $Le = 10$, 2, 0.5 and 0.1, respectively. These figures show that the effect of increasing R_S is to increase R_{Dc} and stabilize the fluid flow. The critical thermal Darcy–Rayleigh number, existing for those values of R_S and Le throughout the range of H, is found to be invariant and approaches different limits at the extreme values of $H << 1$ and $H >> 1$. It is worth mentioning here that the definition of thermal Darcy–Rayleigh number is not the one usually employed when dealing with the LTE situation ($H \to \infty$). In this limit, the LTE definition of thermal Darcy–Rayleigh number is $\tilde{R}_D = \gamma R_D/(1+\gamma)$. The limit $H \to 0$ yields a regime utterly opposite to that of LTE due to the temperature fields of solid and fluid phases being completely independent of this limit. In fact, in the limit of vanishingly small H, the critical thermal Darcy–Rayleigh number attains the lowest (highest) possible values for the onset of instability when the Lewis number $Le < 1 (Le > 1)$. Though Fig. 6a, b exhibit the instability to initiate as the stationary mode for $R_S = 300$ and 500, it switches over to the travelling-wave mode as the value of H reaches some transition value H_T, which gets decreased with increasing R_S. To the contrary, the instability occurs only through the stationary mode for other values of $R_S (= 100, 200)$ throughout the range of H. Figure 6c shows an altogether different behavior. For each value of R_S considered, the R_{Dc} curves of the stationary mode end at some value of H indicating the base flow is asymptotically stable thereafter but with an exception when $R_S = 500$ in which case the instability ensues again via travelling-wave mode after a certain value of H. In other words, there exists a finite range of H in which the flow will be stable for $R_S = 500$. Another point to be noted from this figure is that the flow remains stable for $R_S < 103.45$ and becomes unstable for $R_S \geq 103.45$. This shows that instability exists for a certain parametric space of R_S which prominently depends on Le as observed in the LTE case[28]. Figure 6d exemplifies that the instability appears only in the form of stationary mode for all values of R_S and H considered, while for $R_S = 100$ the curve ceases at some value of H as observed in Fig. 6c. From the figures, it is also obvious that the effect of increasing $Le (> 1)$ is to hasten and on the contrary increase in $Le (< 1)$ is to delay the onset of instability for a fixed value of R_S. One common feature that emanates from these outcomes is that there exists a threshold value of R_S exceeding which only the base flow becomes unstable and below which the flow remains to be stable as observed in the single diffusive component case[19]. The threshold value of R_S is found to depend strongly on the values of other governing parameters. Alter-

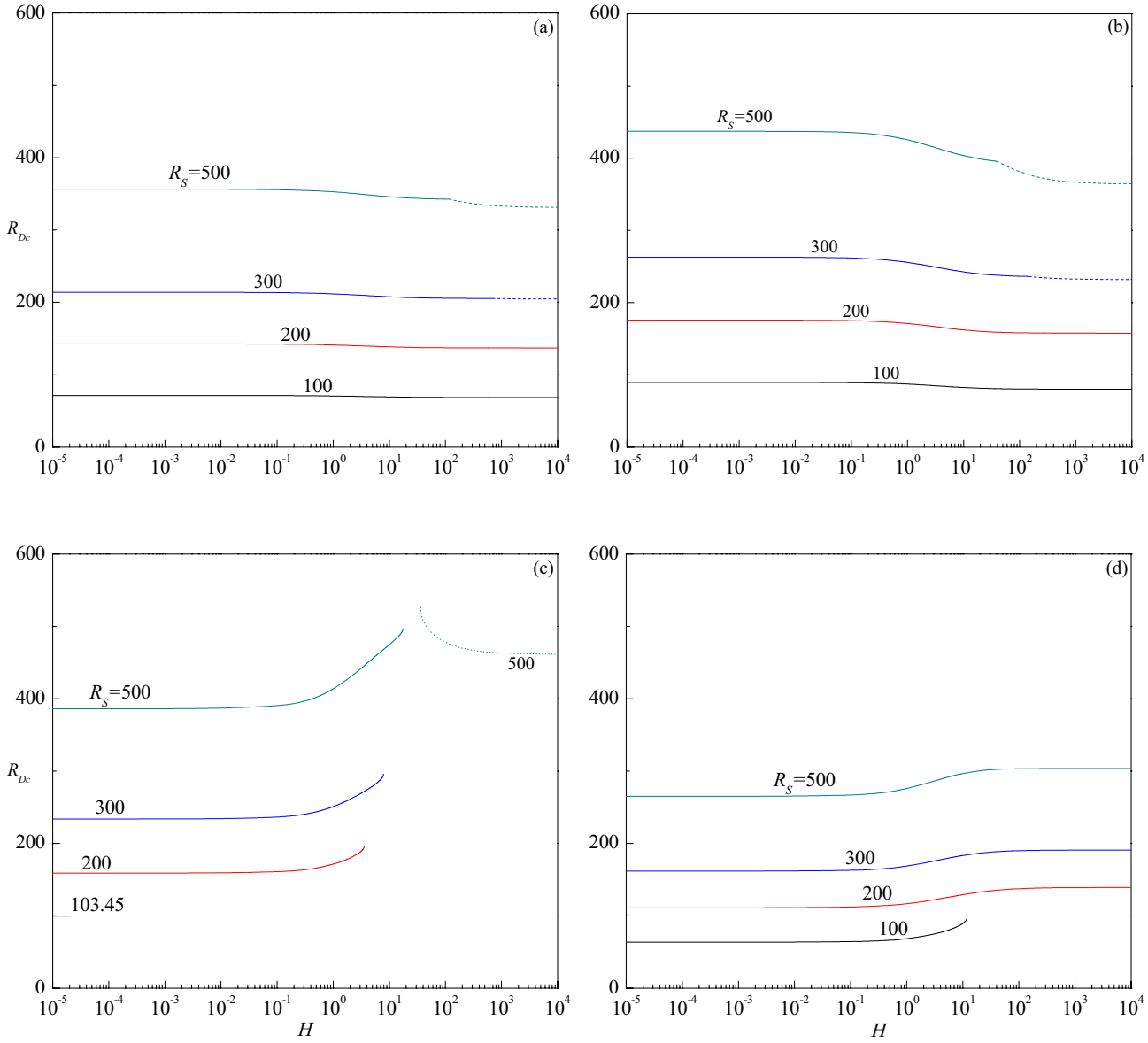

Figure 6. The variation of R_{Dc} versus H for different values of R_S relative to the cases (**a**) $Le = 10$, (**b**) $Le = 2$, (**c**) $Le = 0.5$ and (**d**) $Le = 0.1$, when $\gamma = 1$.

natively, we also considered the plots of critical solute Darcy–Rayleigh number R_{Sc} versus H for different values of R_D for a fixed value of Le (Figures are not shown) to get an insight into the problem. We witnessed that the overall behavior perceived was akin to that of Fig. 6, except the difference in the values of R_{Sc} and R_{Dc}.

The variation of critical wave number a_c with H is presented in Fig. 7a–d for the corresponding parametric values considered in Fig. 6a–d. The figures show that increasing R_S is to decrease a_c in both stationary and travelling-wave modes for all values of Le considered and hence its effect is to enlarge the size of convection cells. Even though the critical wave number of stationary mode increases with H for $Le = 10$, the insignificant variation in its value is apparent from Fig. 7a. However, a_c of travelling-wave mode instability for $R_S = 300$ and 500 initially increases slightly and remains to be constant with H. An opposite trend follows for $Le = 2$ and the changes in a_c with H are somewhat noticeable in the stationary mode (Fig. 7b). Figure 7c displays the results for $Le = 0.5$ and observes a steep increase in a_c of the stationary mode with increasing H except for $R_S = 103.45$. However, a_c increases slightly before attaining a constant value at higher values of H when the instability changes to the travelling-wave mode for $R_S = 500$. The plots of a_c for $Le = 0.1$ increase at the intermediate values of H for all values of R_S but end at some value of H for $R_S = 100$ (Fig. 7d). The figures further disclose that the critical wave number decreases (increases) with increasing $Le > 1$ ($Le < 1$) for each value of R_S. Figure 8a–c show the corresponding change of critical wave speed c_c as a function of H for $Le = 10$, 2 and 0.5, respectively since the instability occurs through the stationary mode for $Le = 0.1$. These figures show an interruption in the curves of c_c with H due to a change in the mode of instability from the stationary mode ($c_c = 0$) to the traveling-wave mode ($c_c \neq 0$). It is also noted that c_c increases with increasing R_S, H and Le, and attains a constant value as $H \to \infty$.

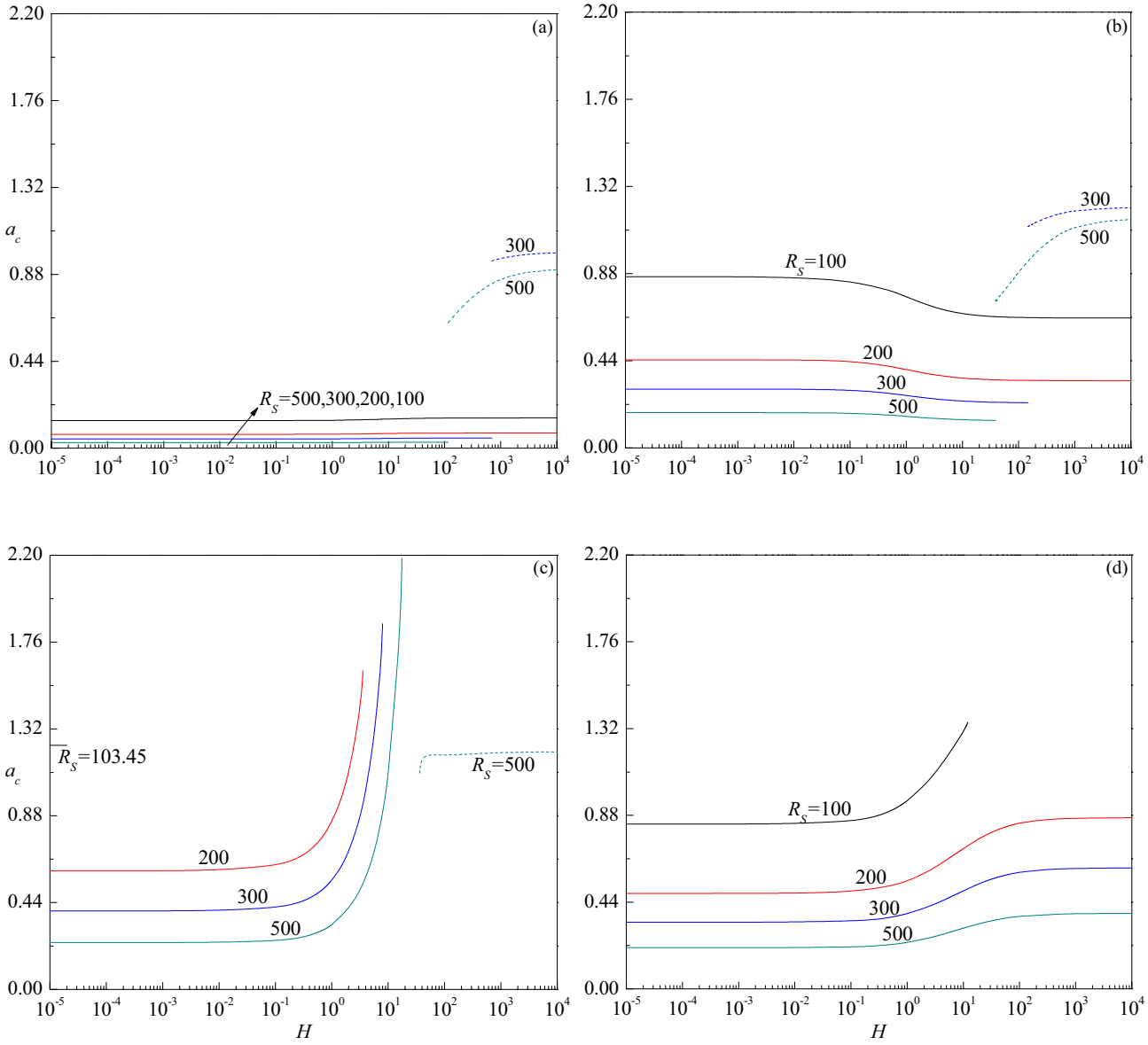

Figure 7. The variation of a_c versus H for different values of R_S relative to the cases (**a**) $Le = 10$, (**b**) $Le = 2$, (**c**) $Le = 0.5$ and (**d**) $Le = 0.1$, when $\gamma = 1$.

Figure 9a–d demonstrate the impact of porosity modified conductivities ratio γ on the variation of R_{Dc} as a function of H for different values of R_S. For $\gamma = 0.01$, it is observed that the instability sets in always via stationary mode throughout the range of H for the values of R_S considered (Fig. 9d). However, depending on the value of R_S, the shifting of instability from the stationary to the travelling-wave mode emerges after certain values of H for $\gamma = 0.1$ (Fig. 9c), 1 (Fig. 9b) and 10 (Fig. 9a). Despite the critical thermal Darcy–Rayleigh number assuming different values at extreme values of $H \to 0$ and $H \to \infty$ for smaller and moderate values of γ (Fig. 9b–d), it becomes independent of H at sufficiently large values of γ (Fig. 9a). This is because, $\tilde{R}_D = R_D$ as $\gamma \to \infty$ and this describes a fluid with an extremely high thermal conductivity. This explains why the temperature of the fluid is not influenced by that of the solid, while the temperature of the solid is locally coincident with that of the fluid. As a result, interphase convection is prevented at the pore level, but extremely efficient heat conduction in the fluid creates a perfect thermal link between the phases. Moreover, both R_{Dc} and a_c become independent of γ at lower values of H as the solid phase does not affect the onset criterion. On the other hand, R_{Dc} and a_c

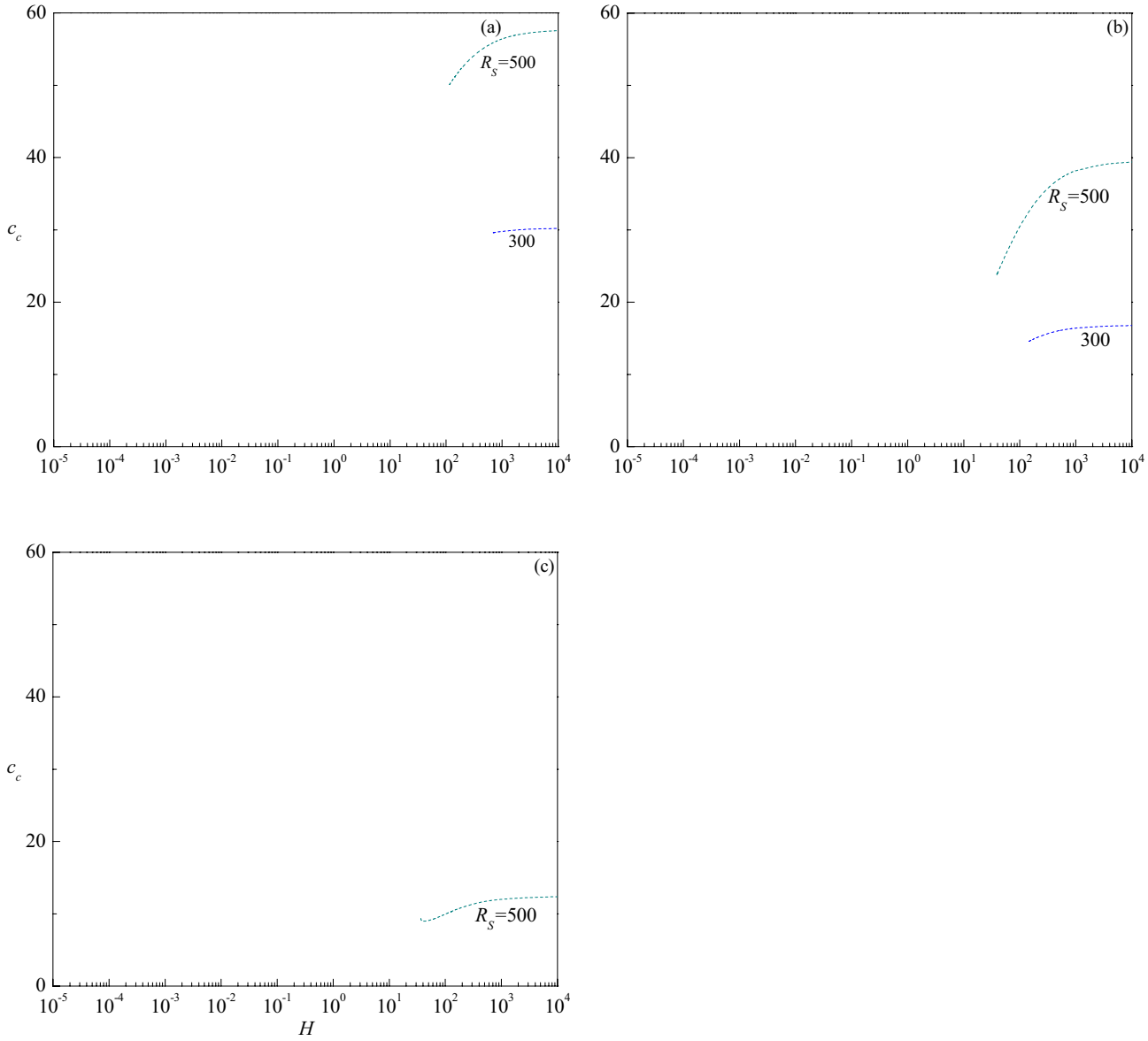

Figure 8. The variation of c_c versus H for different values of R_S relative to the cases (**a**) $Le = 10$, (**b**) $Le = 2$ and (**c**) $Le = 0.5$ when $\gamma = 1$.

varies significantly with γ at higher values of H since the stability criterion depends on the mean properties of the medium. Also, an increase in the value of γ is to increase R_{Dc} indicating its effect is to stabilize the fluid flow (Fig. 9a–d). Whereas, the critical wave number increases with increasing γ at the travelling-wave mode while a mixed behavior could be seen at the stationary mode (Fig. 10a–d). The above observed phenomena are true for all the considered values of R_S. The critical wave speed shows both increasing and decreasing trends with increasing γ (Fig. 11a–d).

Conclusions

The implication of a solute concentration field on the stability of thermal convection in a vertical porous layer subject to different constant temperatures and solute concentrations at the impermeable boundaries is investigated. The Darcy law has been employed in a framework based on the Oberbeck–Boussinesq approximation and the LTNE model has been exploited by assuming two different local temperatures for the fluid and solid phases of the porous medium. To study the stability of the basic flow, a linear stability analysis has been performed by employing a normal mode analysis of the eigenvalue problem. It is observed that the Gill–Rees proof turns out to be ineffective in deciding the stability of the base flow. A numerical analysis has been carried out to extract the critical value of the thermal Darcy–Rayleigh number R_D that identifies the threshold for the onset of instability. It has been established that the second diffusing component evidences a dramatic effect on the stability of the basic flow. A systematic study on the topology of neutral stability curves has been carried out and some remarkable departures from those of LTE regime are observed.

The principal results of the foregoing linear stability analysis can be outlined as follows:

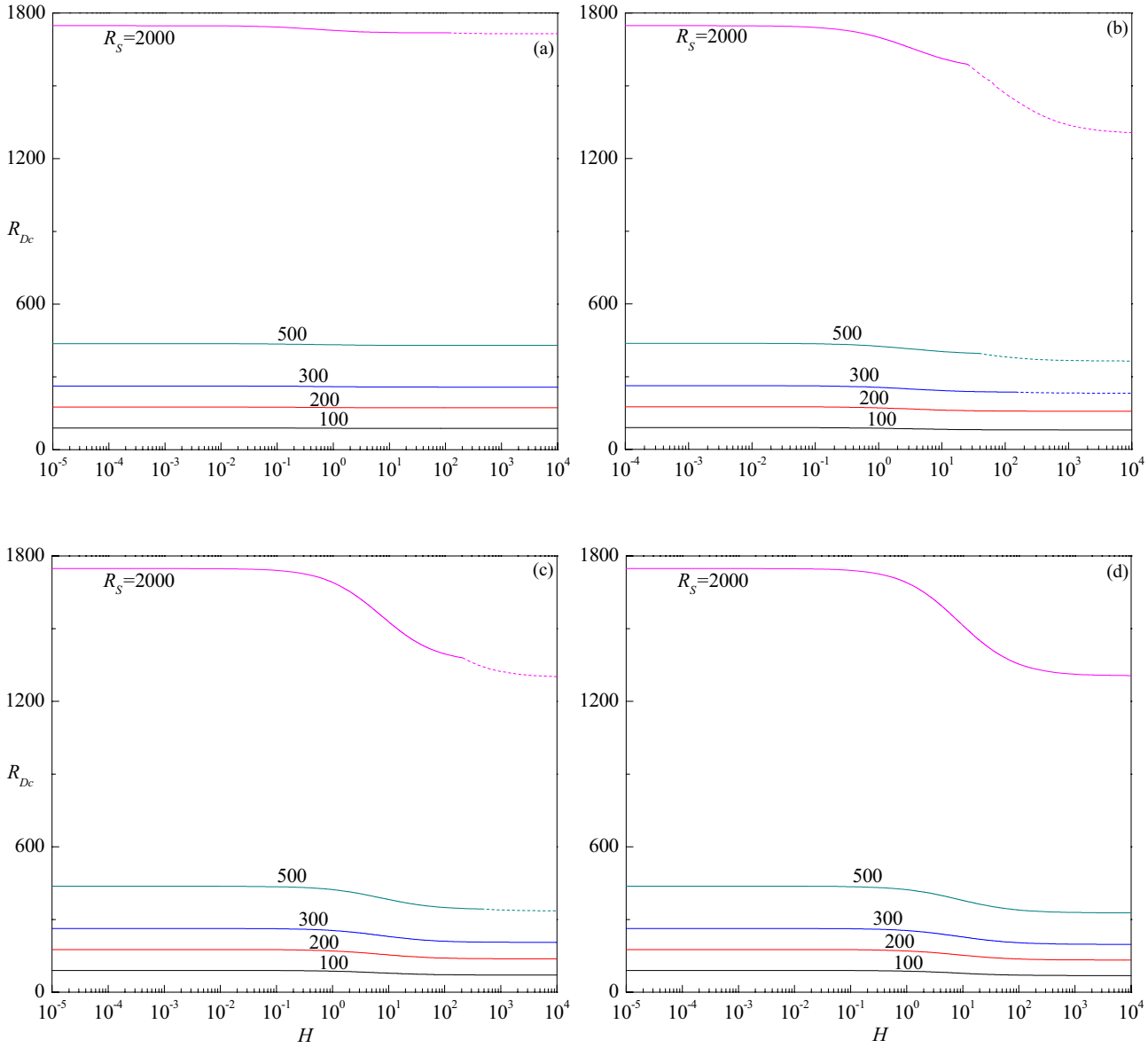

Figure 9. The variation of R_{Dc} versus H for different values of R_S relative to the cases (**a**) $\gamma = 10$, (**b**) $\gamma = 1$, (**c**) $\gamma = 0.1$ and (**d**) $\gamma = 0.01$ when $Le = 2$.

- In contrast to the Gill–Rees stability problem, the presence of a solute concentration field initiates the possibility of base flow becoming unstable under certain parametric conditions.
- Closed neutral stability curves comprising stationary and/or travelling-wave modes exist depending on the choices of governing parameters indicating the requirement of two thermal Darcy–Rayleigh numbers to specify the linear instability criteria instead of the usual single value.
- The mode of instability switches over from the stationary mode to the travelling-wave mode as the local minimum of the neutral stability curve loop formed by these two modes gets interchanged for certain choices of parameters. In particular, the changing over of the preferred mode of instability depends prominently on the value of the scaled interphase heat transfer coefficient H which increases with the decrease in the solutal Darcy–Rayleigh number R_S and an increase in the Lewis number Le. However, a mixed behavior is noticed with an increase in the ratio of porosity-modified thermal conductivities γ.
- The instability of fluid flow is independent of H at its extreme values for all the governing parameters. While the departure from the LTE regime leads to stabilization of the base flow when $Le > 1$ (i.e. thermal diffusivity of the fluid is greater than the thermal diffusivity of the solid), the trend gets reversed when $Le < 1$.
- Increase in R_S, γ and $Le(<1)$ is to abet the stability of fluid flow and exactly an opposite behavior manifests with increasing $Le(>1)$.
- The size of the convection cells increases with increasing R_S and $Le(> 1)$, while it decreases with increasing $Le(< 1)$. A mixed behavior is noticed with increasing γ.

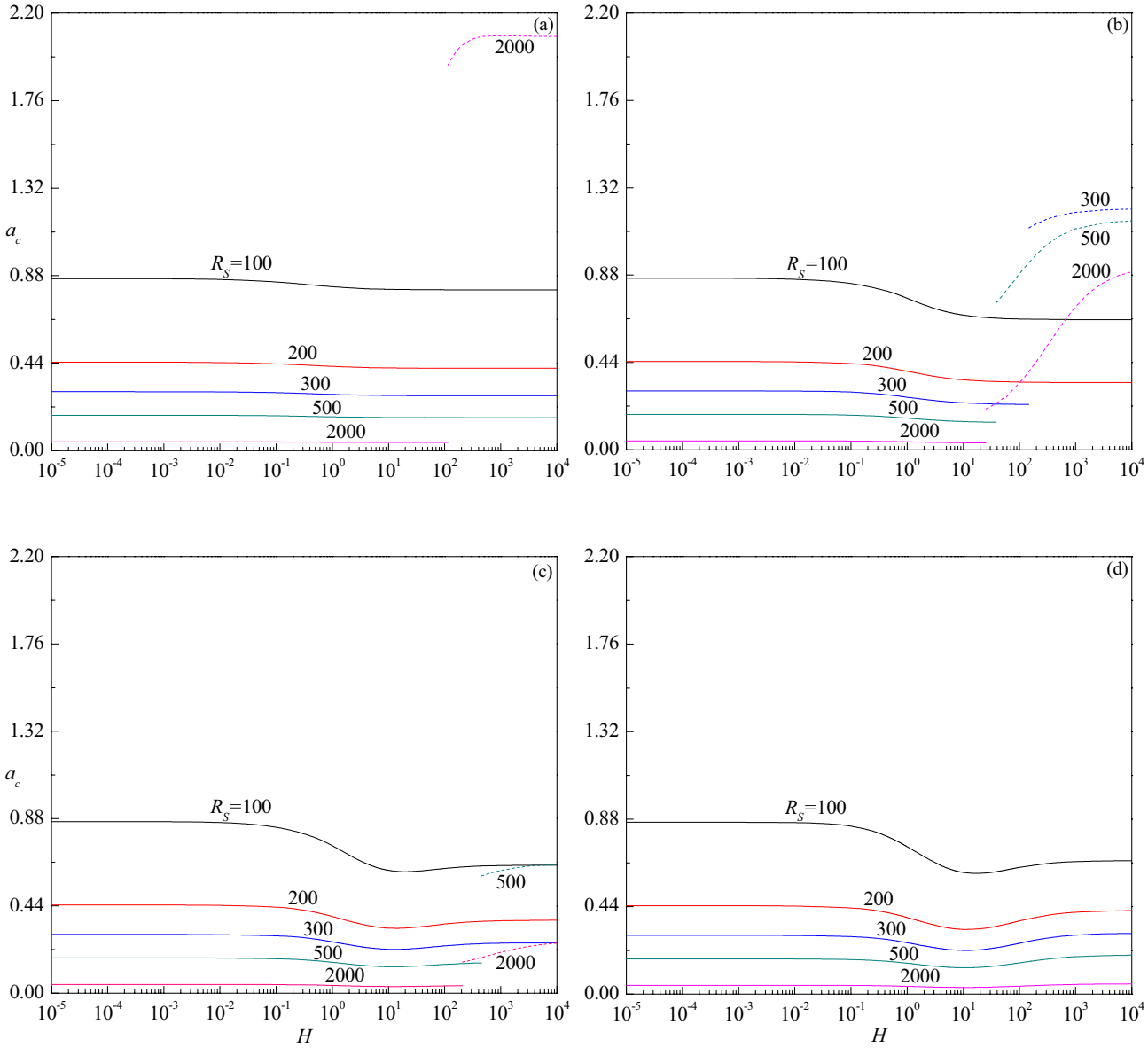

Figure 10. The variation of a_c versus H for different values of R_S relative to the cases (**a**) $\gamma = 10$, (**b**) $\gamma = 1$, (**c**) $\gamma = 0.1$ and (**d**) $\gamma = 0.01$ when $Le = 2$.

We have explored the essence of thermosolutal natural convection through linear stability analysis in a broader context but it also requires further investigation through a weakly nonlinear stability analysis and direct numerical simulation. These analyses give more details about the flow instabilities beyond the small-amplitude stage. Also, one may consider the implications of partially permeable boundary conditions. With such a model, one can investigate the gradual transition from permeable to perfectly impermeable boundaries, and its effects on the onset conditions for the instability. These are left for future study.

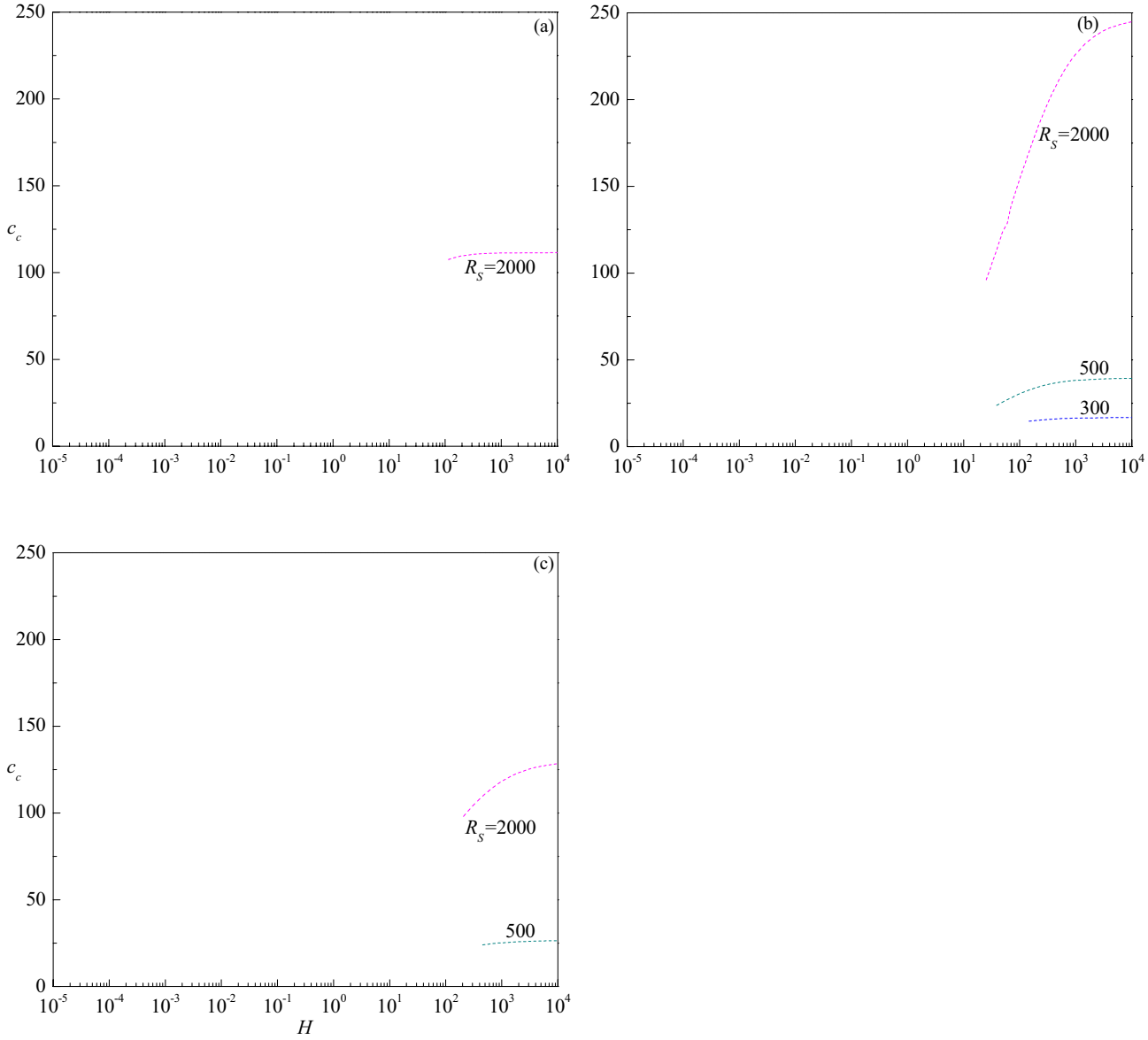

Figure 11. The variation of c_c versus H for different values of R_S relative to the cases (**a**) $\gamma = 10$, (**b**) $\gamma = 1$ and (**c**) $\gamma = 0.1$ when $Le = 2$.

Data availability

The data that supports the findings of this study are available within the article.

Received: 1 February 2022; Accepted: 21 September 2022
Published online: 11 November 2022

References

1. Straughan, B. *Stability and Wave Motion in Porous Media: Applied Mathematical Sciences* Vol. 165 (Springer, 2008).
2. Nield, D. A. & Bejan, A. *Convection in Porous Media* 5th edn. (Springer, 2017).
3. Barletta, A. *Routes to Absolute Instability in Porous Media* (Springer, 2019).
4. Gill, A. E. A proof that convection in a porous vertical slab is stable. *J. Fluid Mech.* **35**, 545–547 (1969).
5. Rees, D. A. S. The stability of Prandtl–Darcy convection in a vertical porous layer. *Int. J. Heat Mass Transf.* **31**, 1529–1534 (1988).
6. Barletta, A. & Alves, L. S. D. B. On Gill's stability problem for non-Newtonian Darcy's flow. *Int. J. Heat Mass Transf.* **79**, 759–768 (2014).
7. Shankar, B. M. & Shivakumara, I. S. On the stability of natural convection in a porous vertical slab saturated with an Oldroyd-B fluid. *Theor. Comput. Fluid Dyn.* **31**, 221–231 (2017).
8. Barletta, A. A proof that convection in a porous vertical slab may be unstable. *J. Fluid Mech.* **770**, 273–288 (2015).
9. Shankar, B. M., Kumar, J. & Shivakumara, I. S. Stability of natural convection in a vertical layer of Brinkman porous medium. *Acta Mech.* **228**, 1–19 (2017).
10. Shankar, B. M., Kumar, J. & Shivakumara, I. S. Boundary and inertia effects on the stability of natural convection in a vertical layer of an anisotropic Lapwood–Brinkman porous medium. *Acta Mech.* **228**, 2269–2282 (2017).

11. Shankar, B. M. & Shivakumara, I. S. Gill's stability problem may be unstable with horizontal heterogeneity in permeability. *J. Fluid Mech.* **943**, A20 (2022).
12. Rees, D. A. S. Microscopic modeling of the two-temperature model for conduction in heterogeneous media: Three-dimensional media. In *Proceedings of the 4th International Conference on Applications of Porous Media*, Istanbul, Paper 15, August 2009.
13. Rees, D. A. S. Microscopic modelling of the two-temperature model for conduction in heterogeneous media. *J. Porous Media* **13**, 125–143 (2010).
14. Calmidi, V. V. & Mahajan, R. L. Forced convection in high porosity metal foams. *J. Heat Transf.* **122**, 557–565 (2000).
15. Zhao, C. Y., Lu, T. J. & Hodson, H. P. Thermal radiation in ultralight metal foams with open cells. *Int. J. Heat Mass Transf.* **47**, 2927–2939 (2004).
16. Sanjuán, N., Simal, S., Bon, J. & Mulet, A. Modelling of broccoli stems rehydration process. *J. Food Eng.* **42**, 27–31 (1999).
17. Zorrilla, S. E. & Rubiolo, A. C. Mathematical modeling for immersion chilling and freezing of foods: part i: model development. *J. Food Eng.* **66**, 329–338 (2005).
18. Dinčov, D. D., Parrott, K. A. & Pericleous, K. A. Heat and mass transfer in two-phase porous materials under intensive microwave heating. *J. Food Eng.* **65**, 403–412 (2004).
19. Rees, D. A. S. The effect of local thermal nonequilibrium on the stability of convection in a vertical porous channel. *Transp. Porous Media* **87**, 459–464 (2011).
20. Scott, N. L. & Straughan, B. A nonlinear stability analysis of convection in a porous vertical channel including local thermal nonequilibrium. *J. Math. Fluid Mech.* **15**, 171–178 (2013).
21. Celli, M., Barletta, A. & Rees, D. A. S. Local thermal non-equilibrium analysis of the instability in a vertical porous slab with permeable sidewalls. *Transp. Porous Media* **119**, 539–553 (2017).
22. Shankar, B. M. & Shivakumara, I. S. Effect of local thermal nonequilibrium on the stability of natural convection in an Oldroyd-B fluid saturated vertical porous layer. *J. Heat Transf.* **139**, 044503 (2017).
23. Shankar, B. M., Shivakumara, I. S. & Naveen, S. B. Impact of thermal non-equilibrium on the stability of natural convection in an Oldroyd-B fluid-saturated vertical porous layer with internal heat sources. *Transp. Porous Media* **133**, 437–458 (2020).
24. Shankar, B. M., Shivakumara, I. S. & Naveen, S. B. Density maximum and finite Darcy–Prandtl number outlooks on Gill's stability problem subject to a lack of thermal equilibrium. *Phys. Fluids* **33**, 124108 (2021).
25. Straughan, B. *The Energy Method, Stability, and Nonlinear Convection. Applied Mathematical Sciences* 2nd edn, Vol. 91. (Springer, 2004).
26. Gershuni, G. Z., Zhukhovitskii, E. M. & Lyubimov, D. V. Thermo-concentration instability of a mixture in a porous medium. *Dokl. Akad. Nauk. SSSR* **229**, 575–578 (English translation *Sov. Phys. Dokl.* **21**, 375–377) (1976).
27. Khan, A. A. & Zebib, A. Double diffusive instability in a vertical layer of a porous medium. *J. Heat Transf.* **103**, 179–181 (1981).
28. Shankar, B. M., Naveen, S. B. & Shivakumara, I. S. Stability of double-diffusive natural convection in a vertical porous layer. *Transp. Porous Media* **141**, 87–105 (2022).
29. Phillips, O. M. *Flow and Reactions in Permeable Rocks* (Cambridge University Press, 1991).
30. Shankar, B. M., Shivakumara, I. S. & Kumar, J. Benchmark solution for the hydrodynamic stability of plane porous-Couette flow. *Phys. Fluids* **32**, 104104 (2020).
31. Shankar, B. M. & Shivakumara, I. S. Stability of Poiseuille flow in an anisotropic porous layer with oblique principal axes: More accurate solution. *Z. Angew. Math. Mech.* **101**, e201900264 (2021).
32. Béghein, C., Haghighat, F. & Allard, F. Numerical study of double-diffusive natural convection in a square cavity. *Int. J. Heat Mass Transf.* **35**, 833–846 (1992).
33. Shankar, B. M., Kumar, J. & Shivakumara, I. S. Stability of double-diffusive natural convection in a vertical fluid layer. *Phys. Fluids* **33**, 094113 (2021).

Acknowledgements

We thank the anonymous referees for suggestions that have led to improvements in the manuscript. One of the authors KVN expresses gratitude to the PES University, India for granting her a fellowship. This research article is dedicated to Dr. M.R. Doreswamy, Chancellor, PES University, on the occasion of his 85th birthday.

Author contributions

All the authors contributed equally to this manuscript.

Funding

B.M.S. gratefully acknowledges the financial support received from the PES University, India through Grant PESUIRF/Math/2020/11.

Competing interests

The authors declare no competing interests.

Additional information

Correspondence and requests for materials should be addressed to B.M.S.

Reprints and permissions information is available at www.nature.com/reprints.

Publisher's note Springer Nature remains neutral with regard to jurisdictional claims in published maps and institutional affiliations.